JOURNAL OF GEOPHYSICAL RESEARCH, VOL. 95, NO. A7, PAGES 10,655–10,670, JULY 1, 1990

Spacelab 2 Electron Beam Wave Stimulation: Studies of Important Parameters

G. D. REEVES[1], P. M. BANKS, T. NEUBERT, AND K. J. HARKER

Space Telecommunications and Radioscience Laboratory, Stanford University, Stanford, California

D. A. GURNETT

Department of Physics and Astronomy, University of Iowa, Iowa City

W. J. RAITT

Center for Atmospheric and Space Science, Utah State University, Logan

The Spacelab 2 space shuttle mission included experiments on the production of waves in the ionospheric plasma by the injection of pulsed electron beams. The Spacelab 2 mission took place during July and August of 1985 and provided an extensive data set which continues to yield new results. The experimental results reported here were obtained with the combined use of the University of Iowa plasma diagnostics package (PDP) and the Stanford/Utah State vehicle charging and potential experiment (VCAP). To date most of the analysis has focused on the sequences performed during the release of the PDP as a free-flying satellite. However, over 300 beam sequences were conducted with the PDP mounted in the orbiter's payload bay. The results of these experiments provide important new information which helps answer some of the outstanding questions which remain. The wave environments which exist in the orbiter payload bay and at several hundred meters away are compared both during ambient conditions and during electron beam injections. The dependence of beam-generated wave characteristics on the duty cycle and the frequency of the pulsed beam are investigated. The duty cycle of the beam is found to be one of the most important parameters affecting the amplitude and the harmonic structure of the waves. Maximum amplitudes are produced by 50% duty cycles and amplitudes are proportional to instantaneous, rather than average, beam current. Harmonic structure also provides insight into the spatial integrity of the propagating beam. The dependence on pulsing frequency is found to show good agreement with theory for whistler mode waves produced through the Cherenkov resonance confirming previous results. Theoretical predictions for the dependence of wave amplitudes on parameters which could not be experimentally investigated are also provided. The results of both the experimental and theoretical studies have important practical consequences for experiments attempting to produce and detect propagating radiation using artificial electron beams.

1. INTRODUCTION

The Spacelab 2 electron beam experiments were part of a long and on-going series of active experiments using electron beams as probes of plasma processes in the ionosphere. Reviews can be found in *Winckler et al.* [1980] and *Reeves* [1989]. Spacelab 2 carried the Stanford/Utah State vehicle charging and potential (VCAP) instruments and the University of Iowa plasma diagnostics package (PDP) as well as a variety of instruments relating to other investigations. The VCAP instruments were designed primarily for the investigation of vehicle charging and return current neutralization processes and descriptions of the instruments and results can be found in *Banks et al.* [1987] and *Hawkins* [1988]. The PDP contained an extensive array of instruments used to study the ambient plasma environment and the modification of that environment caused by the orbiter, its motion through the plasma, its attendant effluents, and the modifications produced by the injection of the electron beam. The PDP instruments are described by *Shawhan et al.* [1984].

The main VCAP instrument of interest in the wave stimulation experiments is the fast pulse electron generator (FPEG). The FPEG produced a 1 keV beam of electrons with a current of 100 mA. It was mounted in a fixed orientation out of the orbiter payload bay, perpendicular to the plane of the wings. The wave receivers are part of the PDP. A single axis electric dipole antenna and a single axis magnetic search coil antenna were connected to a wideband wave receiver. The wideband wave receiver provides wave data with high time and frequency resolution. It simultaneously recorded signals in two frequency ranges. The ELF channel monitored the frequency range 0–1 kHz and the VLF channel monitored the frequency range 0–30 kHz. While the ELF channel recorded 0–1 kHz continuously, the VLF

[1]Now at Earth and Space Science Division, Los Alamos National Laboratory, Los Alamos, New Mexico.

Paper number 90JA00451.
0148-0227/90/90JA-00451$05.00

channel incorporated a frequency switching pattern. The wideband receiver did not record electric and magnetic signals simultaneously. Both included an antenna switching pattern which alternated between the electric and the magnetic antennas every 52 s. As a final point, the ELF and VLF channels each used automatic gain control (AGC) circuits to keep the total output signal strength within strict limits. Each has its own independent AGC.

The PDP and the VCAP instruments were first used together on the space shuttle flight STS 3 in 1982. The FPEG and the PDP instruments were essentially identical to the instruments which were flown on the later Spacelab 2 mission but the PDP was at all times mounted in the payload bay. The wave stimulation experiment results from the STS 3 mission have been presented by *Reeves et al.* [1988*a*]. That investigation established the primary wave responses to the injection of a low power pulsed electron beam. The primary results included (1) pulsed electron beam operation produces both broadband and narrow-band waves, (2) both electric and magnetic wave response is observed, (3) narrow-band waves are produced at harmonics of the pulsing frequency, (4) the harmonic structure varies from one pulsing sequence to another, and (5) narrow-band beam-generated waves are also produced at non-harmonic frequencies and these included "satellite lines" and "subharmonics."

The Spacelab 2 experiments used enhanced experimental and analytic techniques to continue this investigation. Over 300 separate electron beam experiments were performed. Two of the most important were the so-called "Pulsed" and "DC" flux tube connection sequences which provided information on the wave response at distances from the beam of $\approx$ 5–250 m during a six hour free flight of the PDP. Observations of wave fields produced by electron beam operations during the free flight of the PDP using the wideband receiver have been reported by *Bush et al.* [1987], *Reeves et al.* [1988*b*], and *Neubert et al.* [1988, 1990].

Analysis of the wideband wave receiver data after the mission was aided by the development of an algorithm to extract absolute wave amplitudes from the wideband receiver data using information on the gain applied to the signals by the AGC. (See *Reeves* [1989] or *Reeves et al.* [1990].) This capability allowed more quantitative analysis of the data from Spacelab 2 than was possible for STS 3. The primary results from the investigations during the free flight of the PDP were (1) the amplitudes of the beam-generated ac fields were determined, (2) an electromagnetic component of both the broadband and the narrow-band radiation was observed, (3) this component was determined to be whistler mode radiation produced through the Cherenkov resonance. *Gurnett et al.* [1986] and *Farrell et al.* [1988] used filter bank data to identify a funnel-shaped emission between the lower hybrid frequency (ω_{LHR}) and the electron cyclotron frequency (ω_{ce}) as quasi-electrostatic whistler mode waves with wave normal angles near the resonance cone. *Reeves et al.* [1990] used wideband receiver data to show that broadband and narrow-band waves observed below $\approx$ 30 kHz were whistler mode waves with wave normal angles in the central hump of the index of refraction surface (e.g., the wave normal angle is less than the Gendrin angle [$\theta < \theta_G$]).

2. Payload Bay Sequences

Investigations of wave generation during the free flight of the PDP yielded important information about electron beam wave generation. The experiments were carefully coordinated and provided unique data on the wave environment at a variety of locations with respect to the orbiter and the beam for several different FPEG operations. However, the free flight was not the only period which produced interesting data. Literally hundreds of separate FPEG modulation sequences were conducted while the PDP was mounted in the orbiter's payload bay. The results of these investigations are the subject of this paper.

The FPEG was command controlled and could be operated in either preprogrammed modes or through up-linked commands. Operation in preprogrammed modes was the most common and typically several modes were programmed back-to-back in what are referred to as "beam sequences." An interval of FPEG operation at a particular frequency and duty cycle is referred to as a "pulsing period" (which should not be confused with the period of the square-wave modulation). A pulsing period could have a duration of microseconds to minutes but was typically several seconds long. Frequencies were typically several tens of hertz to several tens of kilo-hertz. The FPEG was square-wave modulated and the ratio of the on time of a single pulse to the period between pulses is defined as the duty cycle and could range from nearly 0% to 100%. A beam sequence could consist of one or several pulsing periods. For sequences comprised of several pulsing periods the frequency and duty cycle were varied from one pulsing period to the next in order to investigate specific phenomena.

Figures 1–5 show the beam sequences which are most important to this investigation. The upper plot in each figure shows the frequency of each pulsing period. The lower plot shows the duty cycle for each pulsing period. Duty cycle is plotted relative to 50% (which represents equal beam-on and beam-off times) for reasons which will become apparent. Although, on these plots, each pulsing period is shown with a gap between it and the next this is just for visual clarity. In fact, each pulsing period occurred immediately after its predecessor with no FPEG-off interval between them.

Figure 1 shows one such sequence; the Duty 41 sequence. In this sequence there are 10 pulsing periods. During the first two periods the FPEG is pulsed at 3.9 kHz and the FPEG is operated in pairs of pulsing periods with successively descending frequencies — 3.9 kHz, 976 Hz, 244 Hz, 122 Hz, and 31 Hz (Figure 1a). The first period in each pair has a duty cycle of 4/5 or 80% and the second has a duty cycle of 1/5 or 20% (Figure 1b). Each period has a duration of 10 s. The Duty 21 sequences were similar to the Duty 41 sequences but the frequencies were 3.25 kHz, 814 Hz, 203 Hz, 102 Hz, and 25 Hz and the duty cycles were 2/3 (67%) and 1/3 (33%) (Figure 2). The Duty 41 and Duty 21 sequences were designed to investigate the dependence of the wave characteristics on the duty cycle of the beam pulses to determine if the length of beam on-time affected the characteristics of the waves.

The Beam Energy sequences are depicted in Figure 3. In these sequences the pulsing frequency was held roughly constant (between $\approx$ 500–600 Hz) for each of the 19 pulsing periods while the duty cycle was varied from 0.2% to 99.8%. The beam energy sequences investigated the dependence on the total average current injected by the beam. Note that the twelfth pulsing period in the sequence does not follow the steady progression of duty cycles. Rather, it repeats pulsing period 8 in order to check that there is no systematic change

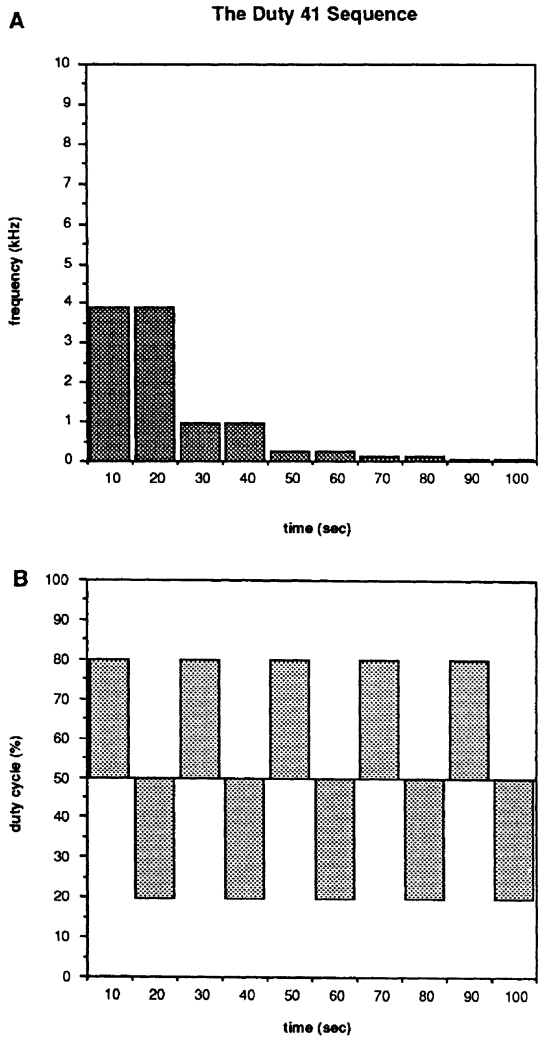

Fig. 1. A schematic representation of the Duty 41 beam sequence. (a) The frequency of the various pulsing periods. (b) The duty cycle of the various pulsing periods. The duty cycles are plotted relative to 50% because the wave response is symmetric about this value (see text). Although they are drawn with a gap between them the actual pulsing periods in a beam sequence took place back-to-back with no FPEG off time between them.

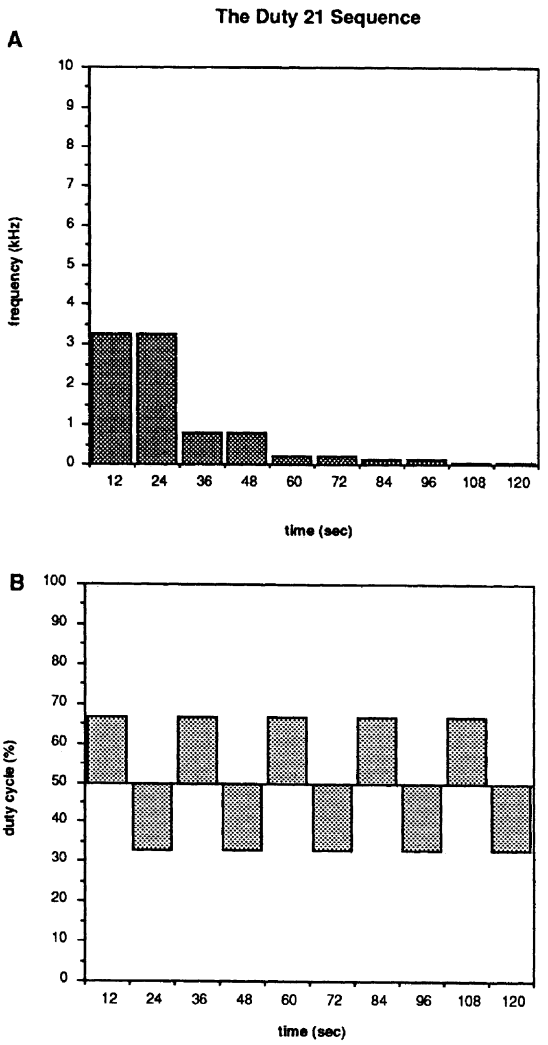

Fig. 2. Similar to Figure 1, this figure shows the pulsing periods for the Duty 21 sequence.

in wave amplitudes due to effects other than changing duty cycle.

The ELF Sweep sequence is shown in Figure 4. The frequency is increased from 51 Hz to 976 Hz in nine steps. At each step the pulsing frequency is increased by approximately a factor of two. The duty cycles of 20%, 33%, or 50% were chosen to be as constant as possible while obtaining the desired frequencies. After nine steps the pattern is repeated twice for a total of 18 pulsing periods. The VLF Sweep sequence (Figure 5) was similar to the ELF Sweep sequence but was designed to span the 0–10 kHz range. The primary purpose of these sequences was to investigate the dependence of wave emissions on beam pulsing frequency and in particular to look for cut-offs or resonances in the wave mode at characteristic wave frequencies.

The Duty 41 and Duty 21 sequences were conducted 17 and 15 times respectively. There were 17 Beam Energy sequences, 10 ELF Sweep sequences, and 28 VLF Sweep sequences. This study concentrates on the results of these five types of beam sequences. In addition there were 13 other types of FPEG sequences whose purposes included study of spacecraft charging and operations attempting to propagate radiation to remote receivers on the ground and on the DE satellite.

3. Comparison of Free Flight and Payload Conditions

During the payload bay wave generation sequences (referred to here as simply "payload bay sequences") the PDP

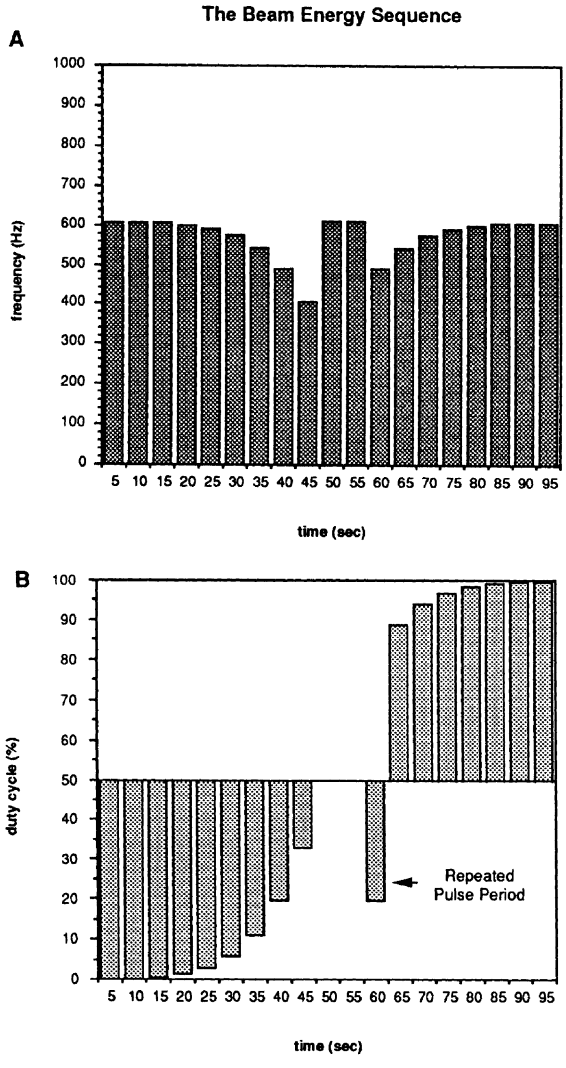

Fig. 3. Similar to Figure 1, this figure shows the pulsing periods for the Beam Energy sequence.

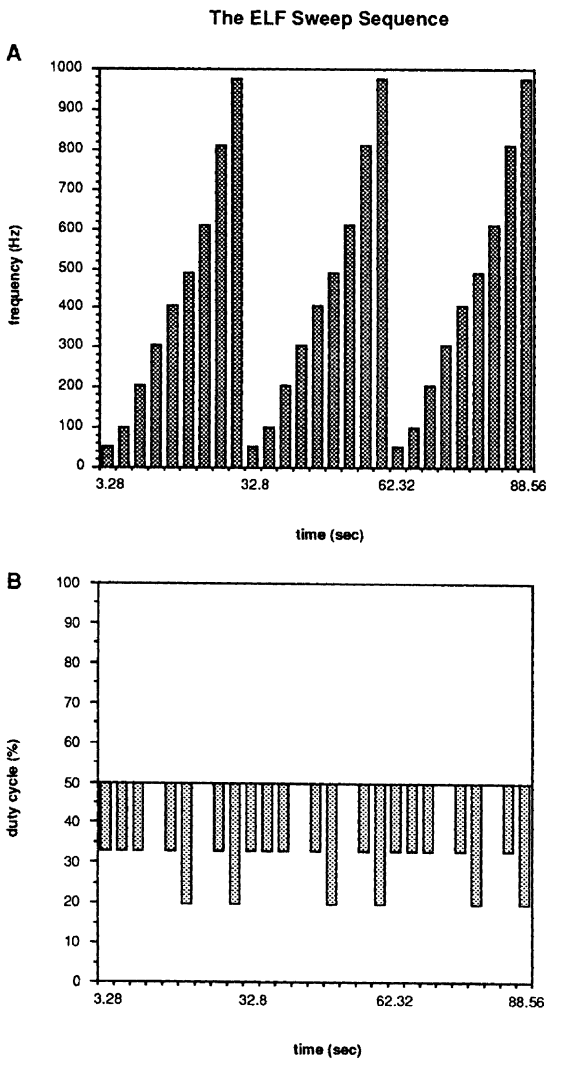

Fig. 4. Similar to Figure 1, this figure shows the pulsing periods for the ELF Sweep sequence.

was located 6.62 m from the FPEG in the orbiter payload bay. Figure 6 shows the relative locations of the FPEG, the PDP, and several other instruments in the Spacelab 2 payload bay. Both the plasma and the ambient wave environments can be quite different in the payload bay than they are at some distance from the orbiter. (See for example *Raitt et al.* [1987], *Shawhan et al.* [1984], and *Hastings et al.* [1988].) Therefore data taken with the PDP in the payload bay are somewhat different than data acquired during the free flight. Most noticeable is the level of background electromagnetic interference (EMI). The interaction of the orbiter moving at $\approx$ 7.7 m/s through the plasma and the presence of on-board electrical systems create both broadband and narrow-band EMI. Vehicle outgassing, thruster operation, and waste releases can introduce new ion species into the environment, vehicle charging can introduce potential structures around the orbiter, and ram/wake conditions can provide dramatically different plasma densities than in the surrounding medium. Although these phenomena are generally assumed to have an effect on the production of waves by electron beams, the magnitude of those effects is not completely understood. It will be seen below that these effects do not substantially alter the basic characteristics of the electron beam-generated waves. Therefore, for the purposes of this investigation, the payload bay can be thought of as similar to, but more noisy than, the undisturbed, ambient plasma environment.

Figures 7–10 show spectrograms produced from the magnetic wideband receiver data. They illustrate both the similarities and the differences between the waves observed during the free flight and during payload operations. All four spectrograms show data in the range 0–30 kHz. The first

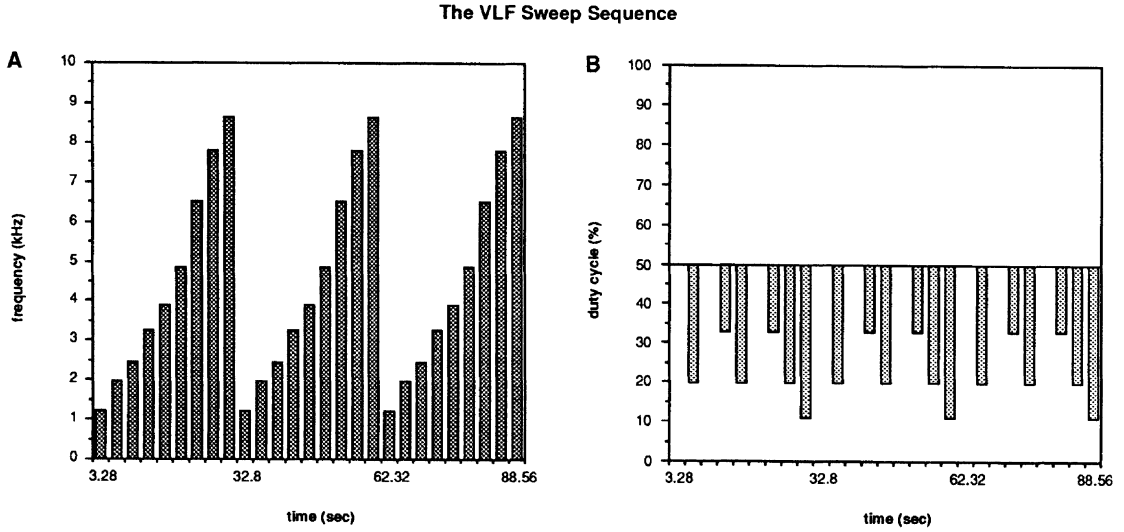

Fig. 5. Similar to Figure 1, this figure shows the pulsing periods for the VLF Sweep sequence.

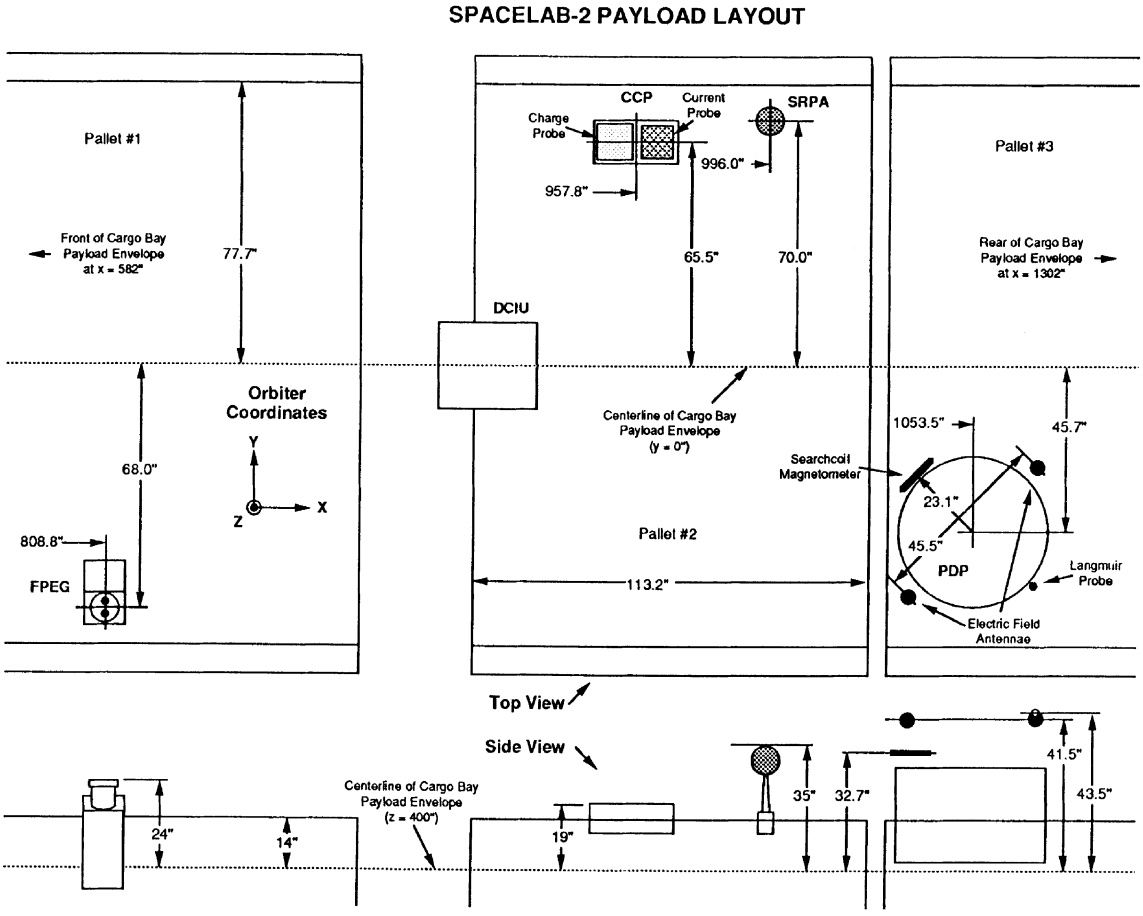

Fig. 6. The location of various VCAP and PDP instruments in the Spacelab 2 payload bay.

$\approx$ 26 s of each shows the 0–10 kHz range. The next $\approx$ 13 s shows the 10–20 kHz range which was heterodyned down into the 0–10 kHz band. The frequency is also inverted in this range so 10 kHz is at the top of the scale and 20 kHz in at the bottom. In the final $\approx$ 13 s the 20–30 kHz range is shown with 20 kHz at the bottom of the scale and 30 kHz at the top. The spectrograms shown here are uncalibrated data. The dynamic effects of the gain applied by the AGC have not been removed and therefore amplitudes are relative. (*Reeves et al.* [1988*a*,1988*b*] show other spectrograms from the Spacelab 2 mission and describe the format in more detail.)

Figure 7 shows the ambient wave environment during the free flight of the PDP. The FPEG is not operating at this time and the PDP is $\approx$ 200 m from the orbiter. Highly time varying emissions are observed in the 0–10 kHz range. Most are natural atmospherics such as whistlers but some are effects of orbiter thruster operations which were frequent during the free flight. In the 10–20 kHz and 20–30 kHz ranges strong interference lines dominate. The line at $\approx$ 11.4 kHz is most likely a source on the PDP because its amplitude is always on the order of 10^{-4} nT. The line at $\approx$ 24 kHz is mostly likely a source on the orbiter. It shows modulation at the spin period of the PDP ($\approx$ 6.5 s for a half rotation) and varies in amplitude with the location of the PDP with respect to the orbiter.

The latter half of the spectrogram in Figure 8 can be compared with Figure 7. During the first $\approx$ 28 s the FPEG is operated in a VLF Sweep sequence. During the remainder of the interval shown the FPEG is off and background fields as measured in the payload bay are shown. It is apparent that in the payload the level of EMI is significantly higher than it is at several hundred meters from the orbiter. The interference lines at $\approx$ 11.4 kHz and $\approx$ 24 kHz are still present and have the comparable amplitudes as were observed near the beam during the free flight. In addition a multitude of other interference lines are also observed with comparable amplitudes. Some of the sources can be identified. For example, harmonics of 60 Hz and 400 Hz (the orbiter power converter frequency) are common.

Figure 8 also shows the response to FPEG operations as measured from the payload bay. Pulsing periods during a VLF Sweep sequence with frequencies 1.95 kHz to 8.65 kHz are seen in the 0–10 kHz range. The final pulsing period at 1.22 kHz starts in the 0–10 kHz range and continues as the antenna switches to the 10–20 kHz range. The sequence is prematurely terminated after this pulsing period. It is seen that the narrow-band magnetic wave fields produced by the beam are significantly stronger than the background EMI. The gain applied by the AGC at this time is such that essentially only beam-generated waves are measured.

Figures 9 and 10 show the wave response to a pulsing sequence which was conducted both during the free flight (Figure 9) and with the PDP in the payload bay (Figure 10). The FPEG is pulsed at 1.22 kHz with a duty cycle of 50% and a current of 100 mA. This sequence, known as the Proximate Operations sequence is referred to as the "Pulsed flux tube connection" sequence during the free flight and

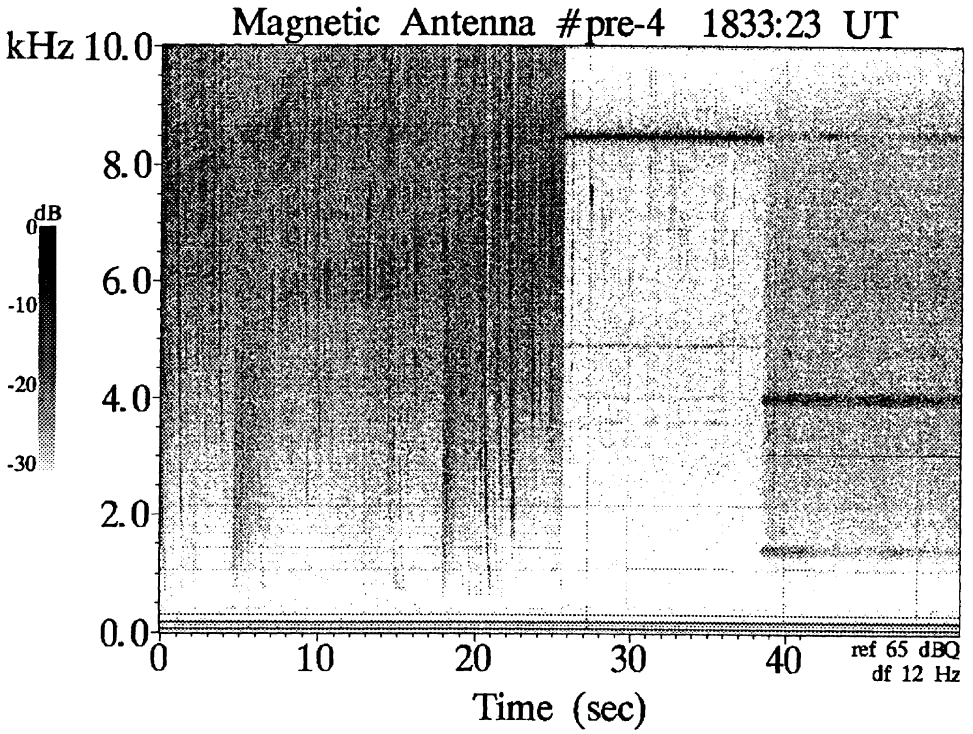

Fig. 7. A spectrogram showing the wave response measured by the PDP magnetic search coil during the free-flight of the PDP. The FPEG is off during this period and ambient fields are measured. The antenna switching pattern and the gain applied by the AGC are both super-imposed on the data.

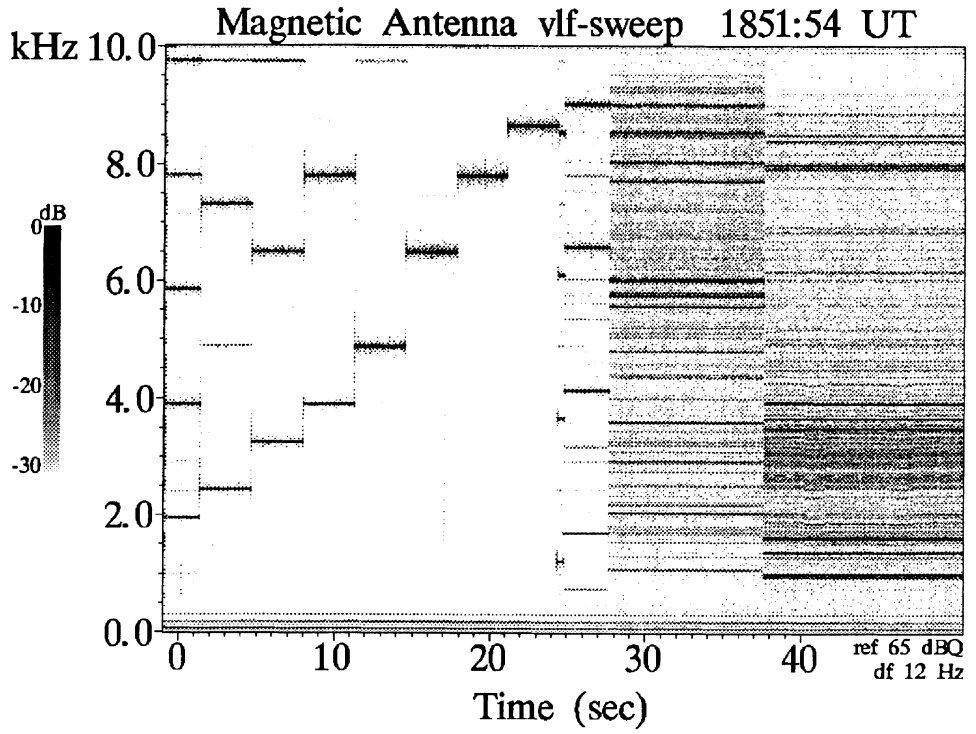

Fig. 8. A spectrogram showing the wave response measured by the PDP magnetic search coil when the PDP is in the payload bay. From ≈ 0–28 s in the figure the FPEG is operated in a VLF Sweep sequence. In the remainder of the figure background EMI is measured.

the "Prox Ops" sequence in the payload bay [*Reeves et al.*, 1988*b*,1990]. The wave response is seen to be nearly identical. Harmonics of the pulsing frequency are observed up to the limit of the receiver. Broadband waves are also generated in both cases but are approximately one to two orders of magnitude lower in amplitude than the narrow-band emissions. In Figure 10 the amplitude of the fundamental is $\approx 5 \times 10^{-3}$ nT and is fairly constant over time. In Figure 9 the amplitude of the fundamental is an order of magnitude lower due to the separation between the PDP and the beam (≈ 70 m). Ambient wave fields are more comparable in amplitude to the beam-generated waves during the free flight even though they are lower in absolute amplitude than the EMI in the payload bay. The other major difference between the two spectrograms is that the free flight signals are modulated by the spin of the PDP while in the payload the PDP is in fixed orientation.

4. Theory of Narrow-band Wave Production

There are several advantages to a pulsed mode of electron beam operation. As seen, pulsed electron beams produce narrow-band emissions at discrete, predictable frequencies. These waves can be readily distinguished from background emissions. In addition pulsing the electron beam produces a current source which can radiate coherently and can therefore produce more intense radiation than an incoherent source [*Bell*, 1968]. As a result there has been considerable effort to develop a theoretical model for wave production by pulsed electron beams.

Harker and Banks [1983] considered the radiation from a finite train of pulses injected into a magnetized plasma. For simplicity, each pulse was assumed to traverse an unbounded path length ($-\infty$ to $+\infty$). Radiation was considered in the frequency range from the lower hybrid frequency to the ion cyclotron frequency. *Harker and Banks* [1985] extended that theory to cover the frequency range below the lower hybrid frequency. They also assumed an infinite train of pulses which were injected into a half space (0 to $+\infty$) which is more appropriate to experiments. A later paper, *Harker and Banks* [1987] considered the near-field radiation from such an electron beam. *Neubert and Harker* [1988] extended this work to include expressions for magnetic field amplitudes. We will review the theory of near-field radiation from a semi-infinite pulsed electron beam propagating in a magnetized plasma in this section. The results of *Harker and Banks* [1987] and *Neubert and Harker* [1988] will be used extensively in this paper. They will often be referred to, collectively, as "HBN."

Other treatments of radiation from electron beams in space plasmas have been presented by *Lavergnat and Lehner* [1984] and *Ohnuki and Adachi* [1984] who consider radiation from pulsed electron beams for the special case of zero pitch angle. *Lavergnat et al.* [1984] have presented results for a sinusoidally modulated beam with arbitrary pitch angle.

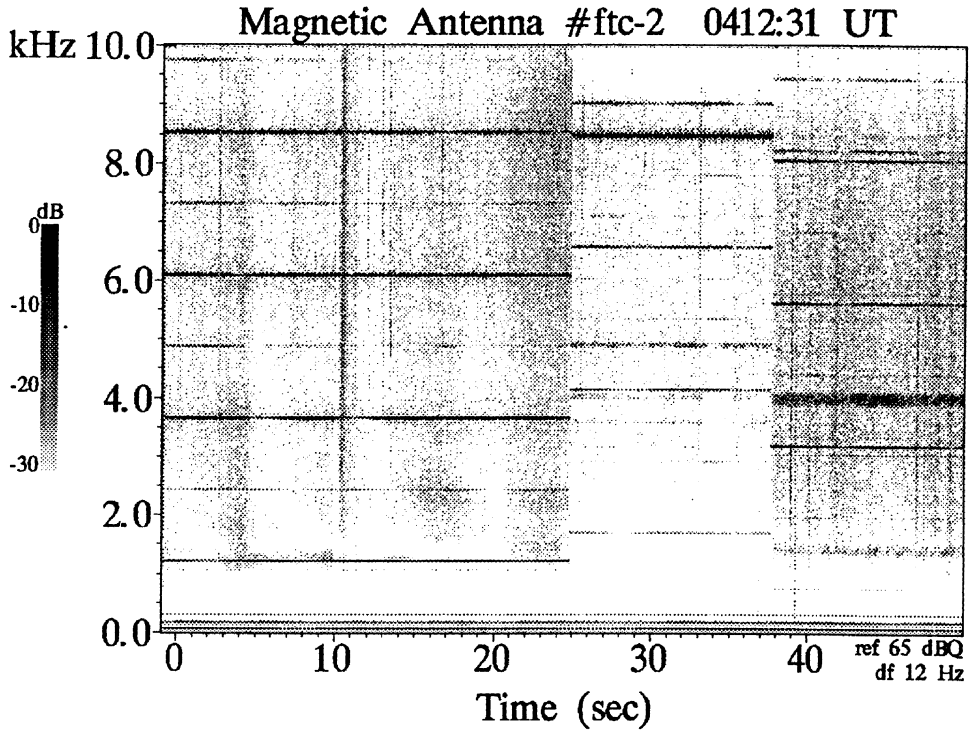

Fig. 9. A spectrogram showing the wave response measured by the PDP magnetic search coil during the free-flight of the PDP. The FPEG is pulsed at 1.22 kHz with a 50% duty cycle. Throughout this interval.

The Theory of HBN

HBN apply a treatment which is based upon the works of *McKenzie* [1967], *Liemohn* [1965], and *Harker and Banks* [1983, and 1985]. They assume an infinitely thin electron beam spiraling around the geomagnetic field (B_0) under the influence of the Lorentz force. The beam is square-wave modulated, (pulsed), and extends into an infinite half space. Within each pulse the electrons are assumed to be evenly distributed and have no motion other than the helical motion of the beam as a whole. Thus such effects as Coulomb spreading of the beam along the magnetic field or across it, are not considered. B_0 is taken to define the z axis of a coordinate system and the electron source is located at (a,0,0) which defines the x axis. (Here, $a = v_\perp/\omega_{ce}$ is the Larmor radius). An exponential attenuation factor, which assumes that the ability of the beam to radiate decays exponentially as $e^{-\beta z}$ over an arbitrary length, $1/\beta$, may also be applied. The factor β could not be estimated for the Spacelab 2 experiments. Therefore we assume here that the coherence length is long and therefore that $\beta \approx 0$.

The electric field and the current density are expressed in a rotating cylindrical coordinate system, Fourier transformed into frequency-wave number space, and the dispersion equation is applied. The fields are then transformed back into coordinate space but are left as functions of frequency. The integrals which must be done are over the components of the wave number vector ($k_\parallel, \phi$, and $k_\perp$). The integral over $k_\parallel$ has simple poles at $n^2 = n_a$, $n^2 = n_b$, and $n^2 = n_\sigma$ where n_a and n_b are functions of the cold plasma dielectric tensor and the perpendicular index of refraction ($\mu_\perp$) and $n_\sigma = (k_{\parallel\sigma}c)/\omega$, where $k_{\parallel\sigma} = (\omega - s\omega_{ce})/v_\parallel$. In addition it has been determined that there is a branch cut whose contribution to the integrals was neglected. The possible effects of this omission will be discussed below.

The reader will recognize the expression for $k_{\parallel\sigma}$ as the familiar resonance condition which picks out the Cherenkov ($s = 0$), cyclotron ($s = 1$), and anomalous cyclotron ($s = -1$) resonances. The cylindrical shape of the beam trajectory naturally leads to the use of Bessel functions (J) and Hankel functions (H). After transforming the fields back from rotating to polar coordinates the final expressions for the electric field components are obtained and are given in *Harker and Banks* [1987]. Magnetic field components are obtained through the relation $\nabla \times \mathbf{E} = -\partial \mathbf{B}/\partial t$. They are given in *Neubert and Harker* [1988]. The reader is referred to those papers for the exact expressions.

Each component of the magnetic fields can be written as

$$B_i = C \sum_{\eta=-\infty}^{\infty} \sum_s \sum_\nu \sum_q \mathcal{D}\,\mathcal{F}\,\mathcal{G}$$

The electric field components have similar form. The subscript i is over the polar coordinates (ρ, ψ, z). C is a constant which includes the factor $\omega_m I_B v_\perp/v_\parallel$ where ω_m is the beam modulation frequency, I_B is the instantaneous beam

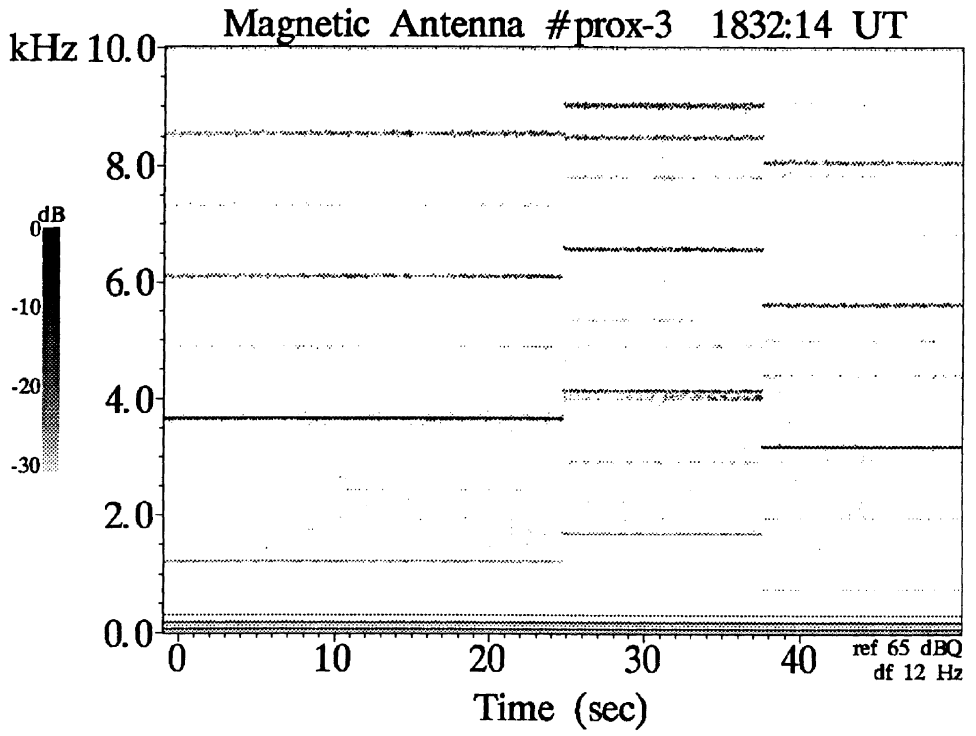

Fig. 10. A spectrogram showing the wave response measured by the PDP magnetic search coil with the PDP in the payload bay. The FPEG is pulsed at 1.22 kHz with a 50% duty cycle. Throughout this interval.

current, and $v_\perp$ and $v_\parallel$ are components of the beam velocity. The summations are over the harmonic number η, the resonance condition s, a spatial coordinate index ν, and an index q which is used to insure that waves are outgoing. The function $\mathcal{G}$ contains factors which depend on the index of refraction and the dielectric tensor elements and also contains the Hankel functions $H_j^{(2)}(\mu_\perp k_0 \rho)$ where $j = s$, $s+1$, or $s-1$. The function $\mathcal{F}$ includes the Bessel function $J_{s-\nu}(\mu_\perp k_0 a)$. The function $\mathcal{D}$ is what we will call the duty cycle factor, $\mathcal{D} = 1/\eta \sin(\eta \pi b/d)$. Here b/d is the duty cycle where b is the on-time for a pulse and d is the period of the square wave modulation. (We note that equation 36 of *Harker and Banks* [1987] and equation 5 of *Neubert and Harker* [1988] are missing the term $1/\eta$.) The dependences described here will be important when we consider the predictions of this theory.

Applications of the Theory

The expressions for the electric or magnetic field components given by HBN can be evaluated numerically for the specific conditions which existed during the Spacelab 2 experiments. The conditions include frequency, duty cycle, beam current, beam energy, the geomagnetic field vector, the plasma density, and the distance of observation. Given those values, an electric or magnetic field vector can be calculated for each of the resonance conditions and for each of the two complex perpendicular indices of refraction ($\mu_\perp$).

This has been done for the Pulsed flux tube connection during the free flight of the PDP [*Reeves et al.*, 1988*b* and 1990]. The results showed the best agreement between predictions and observations for the $s = 0$ root 2 solutions. The Cherenkov resonance is given by $s = 0$. Root 1 solutions are waves with wavenormal angles near the resonance cone ($\theta \approx \theta_{res}$). They are evanescent below the lower hybrid frequency (f_{LHR}). The root 2 solutions are continuous across f_{LHR} and for $f > f_{LHR}$. Above f_{LHR} they are waves with wavenormal angles in the central hump of the index of refraction surface ($\theta < \theta_G$). For the $s = 0$ root 2 solutions the agreement between predictions and observations was better than a factor of 30 for all harmonics at all distances at which waves were measured. Within the context of this type of experiment this agreement is considered quite good. The predictions for the other resonance conditions disagreed with observations by many orders of magnitude.

Broadband waves generated through the Cherenkov resonance were also observed during the free flight. Root 1 (resonance cone) waves were observed to produce a funnel-shaped feature between the lower hybrid and the electron cyclotron frequencies [*Gurnett et al.*, 1986]. Root 2 (central hump) waves contributed to broadband emissions observed below $\approx$ 30 kHz [*Reeves et al.*, 1990]. No wave fields were observed which suggested measurable contributions from the cyclotron or anomalous cyclotron resonances ($s = \pm 1$). For the narrow-band emissions there appeared to be no measured contribution from the root 1 solutions.

In applying the predictions of HBN to payload bay beam operations we again find no evidence for contributions from the cyclotron or anomalous cyclotron resonances and no predictions are presented here for those solutions. For the Cherenkov resonances we cannot exclude the possibility of both the root 1 and root 2 solutions because of the proximity of the beam and the PDP.

The $\approx$ 7 m separation between the beam and the PDP raises another issue. The wavelength of whistler mode waves generated through the Cherenkov resonance can range from meters to several kilometers. The theory of HBN is fully valid in the near-field of the waves provided the point of observation is outside the beam itself.

Two problems exist when applying the theory of HBN to the results from the payload bay beam operations. The first is that the electron density could not be measured accurately when the PDP was in the payload bay [*Raitt et al.*, 1987]. This is a result of the turbulent conditions produced in the payload bay by the motion of the orbiter through the plasma. Thus an approximate value must be used. The second problem is that the theory of HBN, as it stands, is not complete. As noted above, the contributions to the integrals from the simple poles are included but a contribution from a branch cut was neglected. We have evaluated the contributions from the branch cut in the asymptotic far-field limit. The relative contribution of the branch cut will be greater at larger distances from the beam but its effect at the short distances at which the Spacelab 2 experiments were conducted is not known. Nevertheless the theory of HBN in its present form proved quite useful in the interpretation of the free flight wave stimulation results and lacking a complete theory it will again be used here. We will see that it again shows good general agreement and provides an important framework for the interpretation of the experimental results.

5. The Beam Duty Cycle

The duty cycle of the beam is defined at the ratio of the beam on-time to the period of the beam modulation. It is one of the most easily controlled of the beam parameters and turns out to be one of the most important. The duty cycle controls the spatial structure of the beam. This, in turn, controls the amplitude and the spectral characteristics of the waves generated by the beam.

The duty cycle enters into the equations of HBN through the Fourier integral over the spatial structure of the beam. This implies that the dependence of the amplitude on the duty cycle is relatively insensitive to the details of the theory. In HBN the dependence on the duty cycle is very simple. It appears only in the duty cycle factor, $\mathcal{D} = 1/\eta \sin(\eta\pi b/d)$. The factor $\mathcal{D}$ is the same in the equations for each component of the electric and magnetic field vectors and is independent of the mode of the radiation or the resonance condition.

Variation at the Pulsing Frequency

The duty cycle factor is dependent on both the duty cycle and the harmonic number. We begin by considering the dependence of the amplitude of the fundamental ($\eta = 1$) on the duty cycle. The Beam Energy sequence is particularly well suited to this investigation. The Beam Energy sequence consists of 19 pulsing periods (Figure 3). During the sequence the duty cycle for each pulsing period was increased from 0.2% to 99.8%. The frequency for each pulsing period was kept as constant as possible and ranged between 488–608 Hz. The entire sequence lasted 95 s and the local plasma conditions can be considered constant over this interval. With all other variables held constant the dependence of the amplitude of the fundamental on the duty cycle is simply $\sin(\pi b/d)$.

Figure 11 shows that the measured dependence agrees very well with predictions. The function $\sin(\pi b/d)$ is plotted with a solid curve. The amplitude is normalized to an arbitrary value of 0.1 and plotted on a logarithmic scale. The amplitude of narrow-band waves at the pulsing frequency are taken from the magnetic antenna data during two Beam Energy sequences. Each sequence spans an electric and a magnetic antenna period so the full range of duty cycles cannot be compared in a single sequence. Some care was taken to find two sequences which took place under similar conditions. The sequence labeled "bmn" took place at 1900 UT on day 215 and the sequence labeled "bvd" took place at 1738 UT on the same day. During both sequences the payload bay was in light wake conditions with an ambient magnetic field strength of $B_0 \approx 0.45$ G on the Earth's dayside. The most likely cause of the difference in amplitudes at b/d =20% and 50% is a difference in plasma density. The IRI predicted densities [*Bilitza*, 1986] for the two sequences were 3.5×10^5 and 2.6×10^5 cm^{-3} respectively. The higher amplitude waves are observed for the higher density estimate.

The variation with the duty cycle of the beam can be understood in terms of a physically simple model. For a duty cycle of b/d =0% there is no emitted current and no radiation is expected. For a duty cycle of 100% the beam is on continuously (the dc case) and only broadband waves are emitted. The amplitude of narrow-band radiation is again expected to vanish. The presence of narrow-band radiation depends on periodically changing current densities.

One unanswered question from previous investigations was which portion of the beam pulse was responsible for producing the narrow-band radiation. One might expect radiation from, say, only the leading and trailing edges of each beam pulse in which case the wave amplitude should be independent of the duty cycle. The theory of Harker and Banks

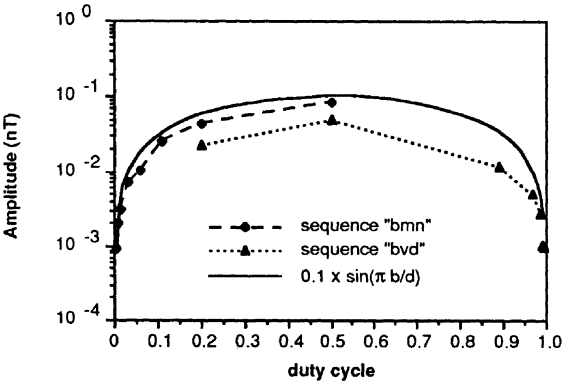

Fig. 11. The variation of the amplitude at the fundamental frequency with duty cycles between 0% and 100%. The solid line is $\sin(\pi b/d)$ arbitrarily normalized to 0.1. Data for two Beam Energy sequences show good agreement with the predicted behavior.

predicts amplitudes based on coherent radiation from the entire length of the pulse. The amplitudes from the Beam Energy sequences indicate that, in fact, the entire pulse radiates. This conclusion is important for understanding the production of narrow-band radiation from pulsed electron beams.

An equally important conclusion is that the amplitude of narrow-band radiation is not dependent on the average current injected by the beam. The beam current which appears in the expressions of HBN is $I_B = -Nev$. N is the density per unit length in a beam pulse and v is the velocity of the beam electrons. Therefore I_B is the instantaneous current when the beam is on (100 mA). The average current is $I_B \times b/d$. The results from the Beam Energy sequence experiments show that a duty cycle of 50% produces the maximum amplitudes even though duty cycles greater than 50% inject larger average currents. These results are expected to be independent of the value of the instantaneous current.

Harmonic Structure and the Duty Cycle Factor

Since the duty cycle factor, $1/\eta \sin(\eta\pi b/d)$, contains the harmonic number, η, the harmonic structure of the observed wave fields is also expected to depend on the duty cycle of the beam. Two major effects are predicted. The first is a decrease in wave amplitude with harmonic number due to the factor $1/\eta$. The second is the exclusion of harmonics for which $\eta b/d$ is an integer. Those harmonics are known as "forbidden harmonics."

Two sequences designed to investigate the variation with duty cycle are Duty 41 and Duty 21 sequences (Figures 1 and 2). Figure 12a shows the harmonic structure for two pulsing periods during a Duty 21 sequence. The pulsing frequency for both periods is 814 Hz. For the Duty 21 sequences the duty cycles were 2/3 and 1/3 or $\approx$ 33% and 67% and for each, every third harmonic is forbidden. Figure 12b shows the predicted variation in amplitude with harmonic number.

Several features are apparent. We note that the tendency is for higher harmonics to appear with lower amplitudes, as expected. The amplitudes of the forbidden harmonics tends to be lower than the harmonics which give nonintegral $\eta b/d$ but are not zero. For both the 33% and the 67% duty cycles, forbidden harmonics are observed with amplitudes up to an order of magnitude above the background noise levels of $\approx 1\text{–}5\times10^{-4}$ nT. These results are consistent with the observations from STS 3 and the Spacelab 2 free flight experiments.

The presence of measurable narrow-band waves at the forbidden frequencies is likely to be the result of loss or partial loss of the spatial coherence of the beam pulses. Figure 13 shows how sensitive the amplitude is to the duty cycle. The predicted amplitude of the second harmonic is plotted for duty cycles in the vicinity of 50%. It is seen that even a 1% change in the actual duty cycle of the beam pulses can result in a substantial and measurable wave amplitude for a forbidden frequency.

An interesting point is that the duty cycle factor is a spatial parameter rather than a temporal one. This is seen in the theory from the fact that the integral which produces the duty cycle factor is over the coordinate space. Evidence of this subtle distinction is also found in the data from the Prox Ops sequence. As mentioned above, the Prox Ops sequence

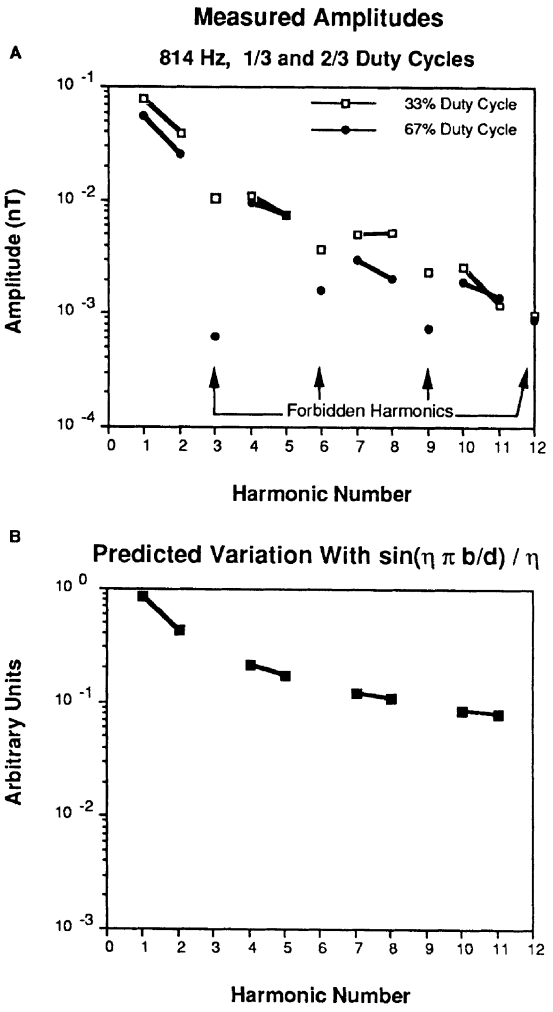

Fig. 12. (a) The amplitude of the harmonics of two pulsing periods during a Duty 21 sequence. The pulsing frequency for both is 814 Hz and the duty cycles are 1/3 and 2/3. (b) The predicted harmonic structure for both pulsing periods ($\sin(\eta\pi b/d)/\eta$).

used a 1.22 kHz pulsing frequency and a 50% duty cycle. It lasted for $\approx$ 10 min. Over this interval the pulsing mode was kept constant but the orientation of the orbiter with respect to the geomagnetic field changed. In the early part of the sequence the beam trajectory was such that it could exit the payload bay freely. Computer simulations have shown that in the later part of the sequence the pitch angle of the beam changed from 120° to 114° from the orbiter z axis and that the electron beam trajectory intersected the orbiter's starboard payload bay door approximately 4 m from the FPEG aperture.

Figure 14 shows the change in harmonic structure. The amplitude of the harmonics of the 1.22 kHz pulsing is shown for two different times. The dark bars show the amplitude when the beam is escaping from the payload bay. The even harmonics are the forbidden harmonics for this sequence and

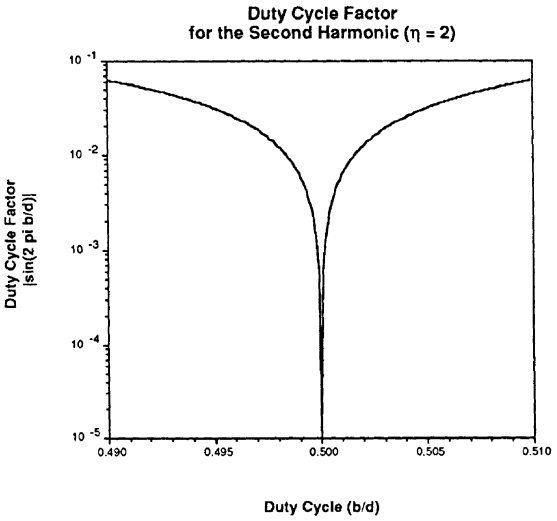

Fig. 13. The duty cycle factor $\sin(\eta\pi b/d)$ for the second harmonic ($\eta = 2$) versus the duty cycle b/d. Very sensitive dependence on the duty cycle is expected. Note the relative values of this factor for duty cycles of 50% and 50.5%.

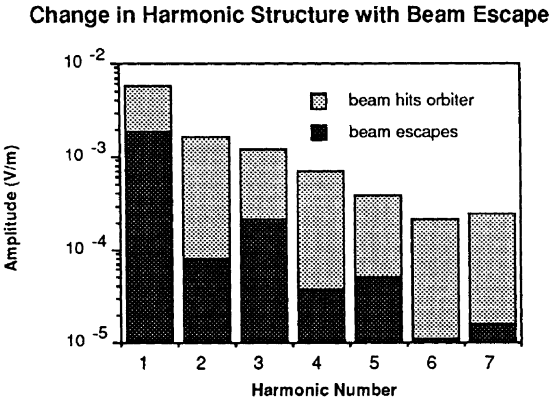

Fig. 14. The harmonics of a 1.22 kHz pulsing with a 50% duty cycle. Dark bars show harmonics with the beam freely escaping the orbiter. Even (forbidden) harmonics have lower amplitudes than odd harmonics. Light bars show harmonics when the beam trajectory hits the orbiter payload bay door. A $1/\eta$ harmonic structure is observed and even harmonics have comparable amplitude to odd harmonics.

they are observed with reduced amplitude compared to the odd harmonics. The light bars show the amplitude when the beam hits the orbiter. The beam is still on for 50% of the time but the length of the beam is essentially restricted to a few meters. In this situation the harmonic structure is roughly $1/\eta$ and the even, forbidden harmonics are of comparable amplitude to the odd harmonics.

There are many factors which could produce a change in the spatial coherence of the beam pulses. As well as the conditions of beam escape, vehicle charging, beam plasma interactions, interactions with return currents, and the Coulomb repulsion of electrons within the beam can produce changes in the effective length of the radiating current source. Any propagation effect which spreads the beam pulses along the magnetic field or retards the leading electrons in a pulse can alter the spatial structure of the current source and hence the physical duty cycle of the beam. Two constraints on any process which can be proposed are (1) that the beam current structure is not drastically different from a square-wave and (2) that the effect on each pulse in the beam is approximately the same since the harmonic structure remains constant over times which are long compared to the duration of a pulse.

6. Variation with the Beam Pulsing Frequency

The other FPEG pulsing parameter which was actively controlled is the pulsing frequency of the beam. The pulsing frequency can be varied over the full 0–30 kHz range of the receiver. The narrow-band structure of the wave response to pulsed electron beams allows specific frequencies to be singled out for investigation. Study of the wave response at the fundamental eliminates the dependence on the harmonic structure of the wave response but does not eliminate the dependence on the duty cycle.

When one considers the plots of predicted amplitude versus frequency presented in *Harker and Banks* [1987] two main characteristics are apparent. (1) The amplitude of the different wave modes ($s = 0, 1, -1$) have very different behavior with varying frequency. (2) Within each wave mode there may be a complex dependence of the wave amplitude on frequency. That dependence includes cut-offs and resonances at characteristic frequencies of the plasma and nulls which are a result of destructive interference in the wave fields. Unlike the dependence of wave amplitude on the duty cycle the dependence on frequency cannot be isolated as a simple factor. Therefore, to examine the dependence of wave amplitude on frequency it is necessary to determine the wave mode and compare observations with the full numerical predictions of HBN.

Figure 15 shows the measured and the predicted variation with the frequency of the pulsed beam. The measured data is taken from an ELF Sweep and a VLF Sweep sequence and is plotted with dots connected by a bold line. The numeric predictions using the theory of HBN are plotted with solid lines. For the predictions a set of "typical" values of various parameters were used. The values for those parameters is given in Table 1 with the exception that both the root 1 (resonance cone) and root 2 (central hump) modes are plotted.

The measurements show the best agreement with the root 2 solutions. The root 1 solutions are predicted to have higher amplitudes than are measured at these distances but do not show the right frequency dependence. These results are the same as the results from the free flight [*Reeves et al.*, 1988*b* and 1990]. The measured values deviate from the predicted amplitudes for the Cherenkov root 2 solutions in two ways. Firstly the behavior of the measured amplitudes at frequencies between 1 kHz and 10 kHz shows two systematic decreases which are not predicted. This is a result of the influence of the duty cycle factor. The predictions are made for a duty cycle of 50%. In the VLF Sweep sequence

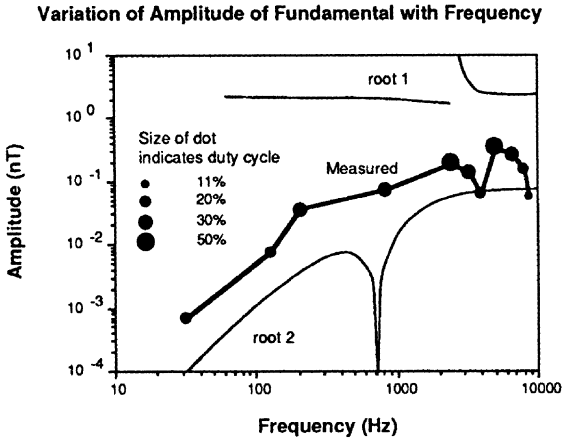

Fig. 15. The variation of the amplitude of the fundamental with the frequency of the pulsing. Predicted curves are shown for the Cherenkov root 1 and root 2 modes (light lines). Measured values are shown for an ELF Sweep and a VLF Sweep sequence (dots connected by bold line). The size of the dot represents the duty cycle for that pulsing period.

the duty cycle ranged from 11% to 50%. The duty cycle for each frequency is represented on the plot by the size of the dot. Frequencies with duty cycles which are less than 50% appear with systematically lower amplitudes. Secondly, the amplitude of the measured amplitudes is consistently higher than predicted. This is most likely due to an inappropriate estimate of the electron density which could not be accurately measured.

7. Predicted Variations with Important Parameters

The duty cycle and the frequency of a particular pulsing period were actively controlled during the Spacelab 2 mission. These two parameters are particularly important in the study of wave generation by electron beam injection. In this section we consider the dependence of wave amplitude on parameters which could not be controlled. Again we use the predictions of HBN. The parameters we will consider are the beam current (I_B), the beam energy (E_B), the geomagnetic field strength (B_0), the pitch angle (ϕ), the ambient electron density (n_e), and the distance from the receiver to the beam ($r_\perp$).

For each calculation a set of default parameters were used (Table 1). Based on the comparison of measured and predicted waves, both during the PDP free flight and with the PDP in the payload bay, we identify the Cherenkov, root 2 (central hump) mode as the most important for these experiments. The beam current and beam energy are the values used for the experiments. For all studies the fundamental frequency ($\eta = 1$) and a duty cycle of 50% are used. The ambient electron density and the geomagnetic field strength are typical values for the experimental conditions. The distance to the beam is defined as the perpendicular distance from the center of the PDP to the center of the beam helix which was typically $\approx$ 5 m for the payload bay sequences. The pitch angle is chosen arbitrarily to be 45°. In each study all the parameters were kept fixed except the parameter being studied. In Figures 16-20 the default value is shown on the axis in bold type. Numerical calculations are presented for pulsing frequencies of 100 Hz, 1 kHz, and 10 kHz.

Table 1. Default Parameters for Predicted Amplitudes

Parameter	Description
resonance condition	Cherenkov (s=0)
mode	root 2 (central hump)
beam current I_B	100 mA
beam energy E_B	1 keV
harmonic number η	1
duty cycle b/d	50%
ambient electron density n_e	10^5cm^{-3}
distance to beam $r_\perp$	5 m
geomagnetic field strength B_0	0.2 G
beam pitch angle ϕ	45°

Beam Current

The dependence of the wave amplitude on the average beam current has already been considered in our discussion of the duty cycle. For the Spacelab 2 and STS 3 missions the instantaneous beam current, I_B was set at 100 mA for all the pulsed beam operations. Figure 16 shows the predicted dependence of wave amplitude on the instantaneous beam current. In the theory of HBN, I_B appears as a constant in the expressions for each of the wave field components. Figure 16 shows the expected linear variation with beam current at all three frequencies (log scale).

Beam Energy

The beam acceleration voltage was 1 kV for all Spacelab 2 FPEG operations. Figure 17 shows the variation in amplitude for beam energies in the range 0–2 keV. The dependence of the expressions for wave amplitude on E_B is primarily a function of the velocity of the electrons. That

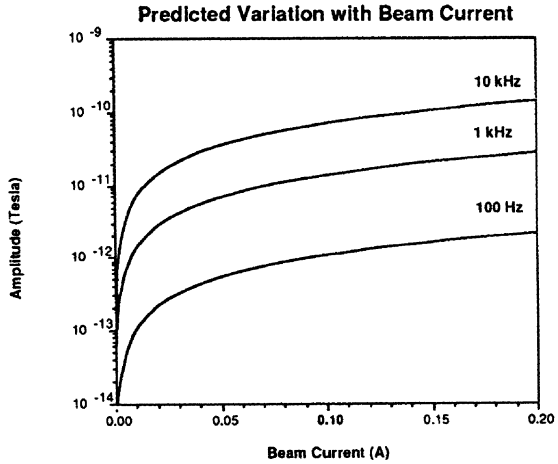

Fig. 16. The predicted variation of amplitude with the beam current, I_B, at frequencies 100 Hz, 1 kHz, and 10 kHz. The default value of 0.1 A is shown in bold type.

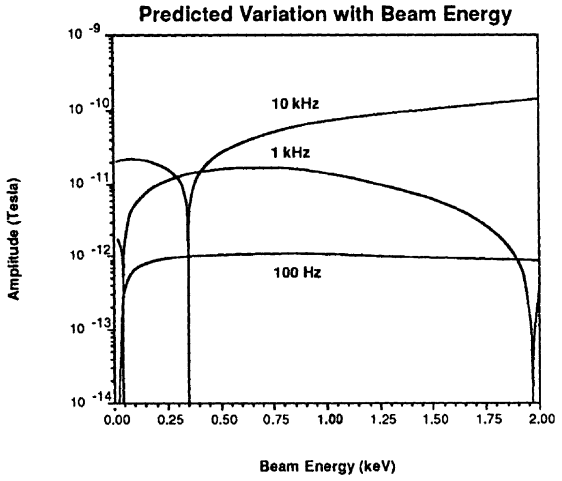

Fig. 17. The predicted variation of amplitude with the beam energy, E_B, at frequencies 100 Hz, 1 kHz, and 10 kHz.

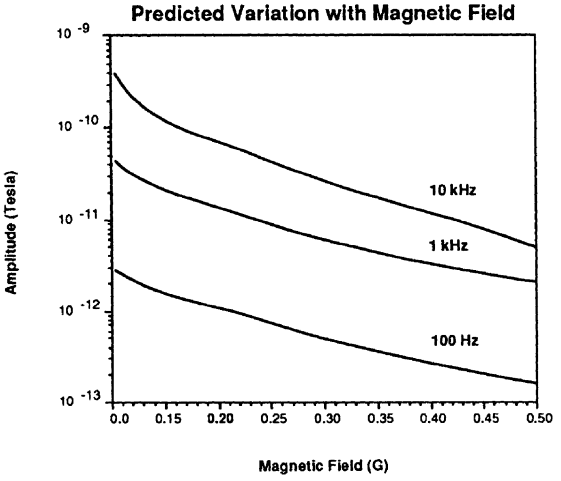

Fig. 18. The predicted variation of amplitude with the geomagnetic field strength, B_0, at frequencies 100 Hz, 1 kHz, and 10 kHz.

velocity, however, determines the gyroradius (which appears in the Bessel functions) and the resonance condition which picks out the values of the parallel index of refraction. Although the dependence of the final expressions on E_B is not simple, the wave amplitudes are predicted to vary little over this range of beam energies.

Although the nominal beam energy for the Spacelab 2 mission was 1 keV it is anticipated that the actual energy of the electrons in the beam could be significantly different. The dynamics of beam escape and the thermalization and Coulomb repulsion of beam electrons are anticipated to change the energy of a substantial population of beam electrons. Figure 17 indicates that changes of energy up to a factor of 2 will not significantly effect the wave amplitudes provided the beam energy alone is changed. Another interesting prediction is that the wave amplitude may actually decrease for higher beam energies at some frequencies.

Geomagnetic Field

The variation with the geomagnetic field strength is shown in Figure 18 . The magnetic field strength determines the characteristic frequencies in the plasma including the electron cyclotron, the ion cyclotron, and the lower hybrid frequencies which in turn appear in the elements of the permittivity tensor and the dispersion relation. B_0 also determines the gyroradius and hence appears in the Bessel functions. Again, in spite of the complex dependence of the field expressions on B_0, the variation over the range $B_0 = 0.1$–0.5 G is fairly smooth and gradual.

The pitch angle (Figure 19) varies significantly in the experiments and can take values in the full range of 0–90°. The pitch angle influences the gyroradius along with B_0 and E_B. It is the dependence of the argument of the Bessel function $(k_\perp m V_\perp / e B_0)$ which causes the nulls in the amplitude seen in the figure. Physically these nulls are caused by destructive interference of waves generated in different parts of the beam. The dependence of the wave amplitude is also seen to be quite different for different frequencies reflecting the

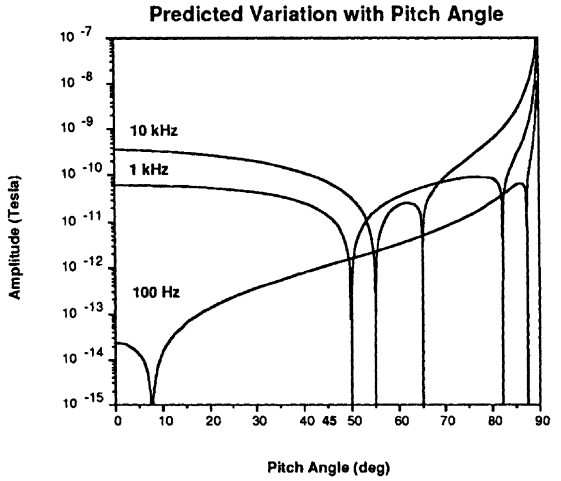

Fig. 19. The predicted variation of amplitude with the pitch angle, ϕ, at frequencies 100 Hz, 1 kHz, and 10 kHz.

dependence of the resonance condition on $V_\parallel$ and hence on ϕ.

We note that the variation of amplitude with pitch angle could provide a very sensitive test of the theory of HBN. The orientation of the FPEG was fixed and therefore on Spacelab 2 the pitch angle was determined by the orbiter orientation with respect to the geomagnetic field. For this reason the Spacelab 2 data set is not adequate for a study of pitch angle variations. Such an investigation may be more easily conducted on a rocket flight.

Electron Density

The local electron density is one of the hardest parameters to determine for sequences in the payload bay because

of the strong and variable effects of ram/wake conditions which may change the plasma density in the payload bay by several orders of magnitude from the ambient levels. The electron density also affects many of the terms in the expressions for the wave amplitudes. It determines the plasma frequencies and the lower hybrid frequency. Therefore it affects the permittivity tensor elements, the index of refraction, and all the terms which depend on them. Those terms include the Bessel function which is again responsible for the nulls in the wave fields plotted in Figure 20. The abrupt drop in wave amplitudes for the 10 kHz predictions at $log(n_e) \approx 5.75$ cm^{-3} is due to the fact that the Cherenkov root 2 resonance condition cannot be satisfied above a critical frequency. This effect was discussed in *Reeves et al.* [1990] in relation to the cut-off in broadband waves during the DC flux tube connection.

Distance

In contrast to the parameters considered above, the dependence on the distance to the electron beam is rather straight forward. In the treatment with no loss of coherence along the path of the beam the distance which is relevant is the perpendicular distance to the center of the beam, $r_\perp$. The perpendicular distance contributes only through the Hankel functions $H_s^{(2)}(\mu_\perp k_0 r_\perp)$ and $H_{s+1}^{(2)}(\mu_\perp k_0 r_\perp)$ and therefore show a smooth decrease with increasing distance.

Although the effect of varying parameters have been considered here individually, under real conditions they are generally observed to vary simultaneously. In addition, the effects of changing a particular parameter may be different at different frequencies. For example, during the free flight of the PDP, as the orbiter moved through space the electron density and the magnetic field strength both vary and as the orbiter maneuvered for the flux tube connections the distance to the receiver and the pitch angle of the beam were altered.

8. Conclusions

Electron beam pulsing sequences conducted with the PDP in the Spacelab 2 payload bay confirm and extend the results of the free flight investigations. The duration of the free flight was 6 hours. Therefore considerably more time was available for experiments when the PDP was in the payload bay. Several distinct beam modulation sequences were designed to investigate the wave response to series of pulsing periods with different frequencies and duty cycles. These sequences include the Duty 41, Duty 21, Beam Energy, ELF Sweep, and VLF Sweep sequences.

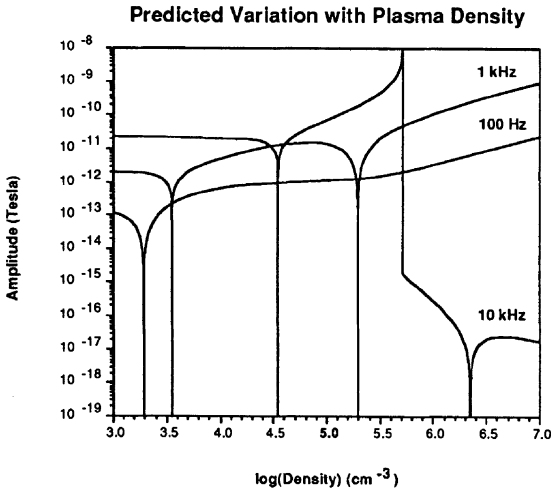

Fig. 20. The predicted variation of amplitude with the ambient electron density, n_e, at frequencies 100 Hz, 1 kHz, and 10 kHz.

The wave environment in the payload bay was compared to that measured during the PDP free flight. The ambient wave fields are found to be quite different. Ambient fields measured several hundred meters from the orbiter consist primarily of natural atmospherics. In the payload bay orbiter-associated EMI dominates the measured fields. In contrast, the beam generated wave response is found to be similar. The most significant differences can be attributed to differences in the position and motion of the PDP relative to the electron beam.

In this analysis the theory of *Harker and Banks* [1987] on wave production by pulsed electron beams is used extensively. Although the theory is not complete it is valid in the near field of the waves and has proven useful for the analysis of free flight and payload bay experiments. Experimental results have shown good agreement with both the qualitative and quantitative predictions of the theory.

The dependence of the narrow-bad wave amplitudes on the duty cycle of the beam has been the subject of extensive investigation. The predicted dependence occurs only in the duty cycle factor $D = (1/\eta)\sin(\eta\pi b/d)$. The results from the Beam Energy sequences show the predicted variation at the fundamental frequency. They establish that the wave amplitude depends upon the instantaneous beam current rather than the average beam current and that maximum wave amplitudes are produced by 50% duty cycles.

The duty cycle is also found to control the harmonic structure of the narrow-band waves. Good agreement with the predicted dependence is observed for all frequencies except at forbidden harmonics. Measured amplitudes at forbidden harmonics are generally lower in amplitude but are not zero. The presence of narrow-band emissions at the forbidden harmonics is attributed to the sensitive dependence of the wave amplitude on the actual spatial extent of the beam pulses.

Investigation of the wave amplitude as a function of beam pulsing frequency also shows good agreement with theory. The dependence on frequency is predicted to be different for the different wave modes. The best agreement s found for the Cherenkov, root 2 solutions in the whistler mode. This is the same conclusion as for the results of the free flight wave experiments.

The beam duty cycle and frequency were actively controlled. Numerical calculations of the expected variation of the wave amplitude with other parameters were also performed. The amplitude of the narrow-band waves are not expected to show strong dependence on the beam current, the beam energy, or the geomagnetic field strength for values of these parameters near the Spacelab 2 conditions. The dependence of the wave amplitude on the beam pitch angle and the ambient electron density is expected to be more complex. In the Spacelab 2 experiments, in general, several parameters varied simultaneously and controlled investigations of a single parameter were not possible. It would be possible in future experiments to actively control the pitch angle and thus keep an important variable fixed or to vary

it in a controlled manner and thus provide a sensitive test of the theory.

Acknowledgments. This work was conducted at Stanford University under NASA grant NAGW-225.

The Editor thanks B. A. Whalen and another referee for their assistance in evaluating this paper.

REFERENCES

Banks, P. M., W. J. Raitt, A. B. White, R. I. Bush, and P. R. Williamson, Results from the vehicle charging and potential experiment on STS-3, *J. Spacecr. Rockets, 24*, 138-149, 1987.

Bell, T. F., Artificial production of VLF hiss, *J. Geophys. Res, 73*, 13, 1968.

Bilitza, D., International reference ionosphere: Recent developments., *Radio Sci., 21*, 343, 1986.

Bush, R. I., G. D. Reeves, P. M. Banks, T. Neubert, P. R. Williamson, W. J. Raitt, and D. A. Gurnett, Electromagnetic fields from pulsed electron beam experiments in space: Spacelab 2 results, *Geophys. Res. Let., 14*, 1015-1018, 1987.

Farrell, W. M., D. A, Gurnett, P. M. Banks, R. I. Bush, and W. J. Raitt, An analysis of whistler-mode radiation from the Spacelab 2 electron beam, *J. Geophys Res., 93*, 153-161, 1988.

Gurnett, D. A., W. S. Kurth, J. T. Steinberg, P. M. Banks, R. I. Bush, and W. J. Raitt, Whistler-mode radiation from the Spacelab 2 electron beam, *Geophys. Res. Lett., 13*, 225, 1986.

Gurnett, D. A., W. S. Kurth, J. T. Steinberg, and S. D. Shawhan, Plasma wave turbulence around the shuttle: Results from the Spacelab 2 flight, *Geophys. Res. Lett., 15*, 760-763, 1988.

Harker, K. J., and P. M. Banks, Radiation from pulsed electron beams in space plasmas, *Planet. Space Sci, 19*, 454-470, 1983.

Harker, K. J., and P. M. Banks, Radiation from long pulse train electron beams in space plasmas, *Planet. Space Sci, 33*, 953-963, 1985.

Harker, K. J., and P. M. Banks, Near fields in the vicinity of pulsed electron beams in space, *Planet. Space Sci, 35*, 11-19, 1987.

Hastings, D. E., N. A. Gatsonis, and T. Mogstad, A simple model for the self-consistent water plasma cloud about an outgassing structure in the ionosphere, *J. Geophys. Res, 93*, 1961, 1988.

Hawkins, J. G., Vehicle charging and return current measurements during electron beam emission experiments from the shuttle orbiter, Ph.D. Dissertation, Stanford Univ., Stanford, Calif., 1988.

Lavergnat, J., and T. Lehner, Low frequency radiation characteristics of a modulated electron beam immersed in a magnetized plasma, *IEEE Trans., AP-32*, 177, 1984.

Lavergnat, J., T. Lehner, and G. Matthieussent, Coherent spontaneous emission from a modulated beam injected in a magnetized plasma, *Phys. Fluids, 27*, 1632, 1984.

Liemohn, H. B., Radiation from electrons in a magnetoplasma, *J. Res. Natl. Bur. Stand., Sect. D 69*, 741, 1965.

McKenzie, J. F., Radiation losses from a test particle in a plasma, *Phys. Fluids, 10*, 12, 1967.

Neubert, T., J. G. Hawkins, G. D. Reeves, P. M. Banks, R. I. Bush, P. R. Williamson, D. A. Gurnett, and W. J. Raitt, Pulsed electron beam emission in space, *J. Geomagn. Geoelectr., 40*, 1221-1233, 1988.

Neubert, T., and K. J. Harker, Magnetic fields in the vicinity of pulsed electron beams in space, *Planet. Space Sci., 36*, 469, 1988.

Neubert, T., K. J. Harker, P. M. Banks, G. D. Reeves, and D. A. Gurnett, Waves generated by pulsed electron beams., *Adv. Space Sci., 10*, 137, 1990.

Ohnuki, S., and S. Adachi, Radiation of electromagnetic waves from and electron beam antenna in an ionosphere, *Radio Sci., 19*, 925, 1984.

Raitt, W. J., J. V. Eccles, D. C. Thompson, P. M. Banks, P. R. Williamson, and R. I. Bush, Plasma parameters in the near wake of the Space Shuttle, *Geophys. Res. Lett., 14*, 359-362, 1987.

Reeves, G. D., P. M. Banks, A. C. Fraser-Smith, T. Neubert, R. I. Bush, D. A. Gurnett , and W. J. Raitt, VLF Wave stimulation by pulsed electron beams injected from the space shuttle, *J. Geophys. Res, 93*, 162, 1988*a*.

Reeves, G. D., P. M. Banks, T. Neubert, R. I. Bush, P. R. Williamson, A. C. Fraser-Smith, D. A. Gurnett, and W. J. Raitt, VLF Wave emissions by pulsed and DC electron beams in space 1: Spacelab 2 observations, *J. Geophys. Res, 93*, 14699-14718, 1988*b*.

Reeves, G. D., Very low frequency radio waves produced by electron beam injection in space plasmas, Ph. D. dissertation, Stanford Univ., Stanford, Calif., 1989.

Reeves, G. D., P. M. Banks, T. Neubert, K. J. Harker, and D. A. Gurnett, VLF wave emissions by pulsed and DC electron beams in space, 2, Analysis of Spacelab 2 results, *J. Geophys. Res, 95*, 6505, 1990.

Shawhan, S. D., G. B. Murphy, J. S. Pickett, Plasma diagnostics package initial assessment of the shuttle orbiter plasma environment, *J. Spacecr. Rockets, 21*, 387, 1984.

Winckler, J. R., The application of artificial electron beams to magnetospheric research, *Rev. Geophys., 18*, 659-682, 1980.

P. M. Banks, K. J. Harker, T. Neubert, and G. D. Reeves, Space Telecommunications and Radioscience Laboratory, Durand 202, Stanford University, Stanford CA 94305.

D. A. Gurnett, Department of Physics and Astronomy, University of Iowa, Iowa City, IA 52242.

W. J. Raitt, Center for Atmospheric and Space Science, Utah State University, Logan, UT 84322

(Received August 22, 1989;
revised January 17, 1990;
accepted February 9, 1990.)